Bubbles in the Near-Surface Ocean: Their Various Structures

JIN WU

Air–Sea Interaction Laboratory, Graduate College of Marine Studies, University of Delaware, Lewes, Delaware

(Manuscript received 8 April 1993, in final form 10 January 1994)

ABSTRACT

Air is entrained by breaking waves to produce bubbles. A highly transient macrobubble cloud is first generated under the breaker, with larger bubbles returning sooner to the sea surface. Those remaining smaller bubbles are then dispersed by near-surface turbulent shear flows in a shallow layer immediately below the undulating sea surface. Bubbles in this layer are shown to be nearly suspended; moreover, vertical distributions of current velocity and bubble concentration within this layer are found to be similar. Both of these features are used to demonstrate that the observed bubble layer, being on the order of 1 m thick, is formed through the longitudinal dispersion process. In addition, isolated microbubble plumes that penetrate several times deeper than the bubble layer appear to be produced also by breaking waves; however, in this case breaking waves temporarily deflect the bubble layer.

1. Introduction

Air bubbles in the ocean are important to many oceanic phenomena, including gas transfer (Thorpe 1982; Merlivat and Memery 1983) and ocean acoustics (McDaniel and Gorman 1983; Farmer and Vagle 1989); they also produce sea spray (Blanchard and Woodcock 1957; Wu 1981a). These bubbles, generated mainly through air entrained by breaking waves, are clustered initially under the breakers and distributed subsequently within a thin layer immediately below the sea surface (Wu 1981b). Temporally averaged data of bubbles reported by several investigators (Kolovayev 1976; Johnson and Cooke 1979; Thorpe 1982; Crawford and Farmer 1987; Walsh and Mulhearn 1987) were parameterized earlier (Wu 1988a, 1992a). In the meantime, the drift currents were found to be also confined within the upper shallow layer (Churchill and Csanady 1983). Taking these findings together, we demonstrate that bubbles in the shallow interface layer are distributed through the longitudinal dispersion process by measured turbulent shear flows. With the understanding gained, we explore observations associated with isolated macrobubble clouds and microbubble plumes before and after, respectively, the bubbles are dispersed within the interface layer and we suggest various effects of breaking waves producing these structures. Dominant sizes of bubbles in the cloud, layer, and plume are also discussed. Most of the processes discussed herein are completed within a few periods of breaking waves; subsequently, Langmuir circulation is believed to be also active to redistribute bubbles already dispersed into the layer (Zedel and Farmer 1991).

Corresponding author address: Jin Wu, Air–Sea Interaction Laboratory, Graduate College of Marine Studies, University of Delaware, Lewes, DE 19958.

2. Shear flows and dispersion processes in the near-surface ocean

a. *Turbulent aqueous flows*

1) TWO COMPONENTS OF DRIFT CURRENTS

The drift currents of a wind-disturbed water surface have two components: wind-induced shear current and wave-induced mass transport (Wu 1975). The former, V_n, was related to the wind stress; experimental results indicated

$$V_n = 0.53\, u_{*a}, \tag{1}$$

where $u_{*a} = (\tau_a/\rho_a)^{1/2}$ is the wind friction velocity, with τ_a being the wind stress and ρ_a the air density. The mass transport, a steady forward motion under surface waves, was theoretically predicted by Stokes (1847) with its maximum value at the water surface

$$V_v = \sigma a^2 k, \tag{2}$$

where V_v is the transport at the water surface, and σ, a, and k are the radian frequency, amplitude, and wavenumber of surface waves, respectively. This expression, as discussed in Wu (1983), has been verified by laboratory measurements.

Using fetch-varied formulas for the wind stress coefficient and surface waves, wind- and wave-induced drift currents at different fetches were estimated by Wu (1983). The results for the wind velocity of 10 m s^{-1} are reproduced in Fig. 1a, in which $V = V_n + V_v$ is the

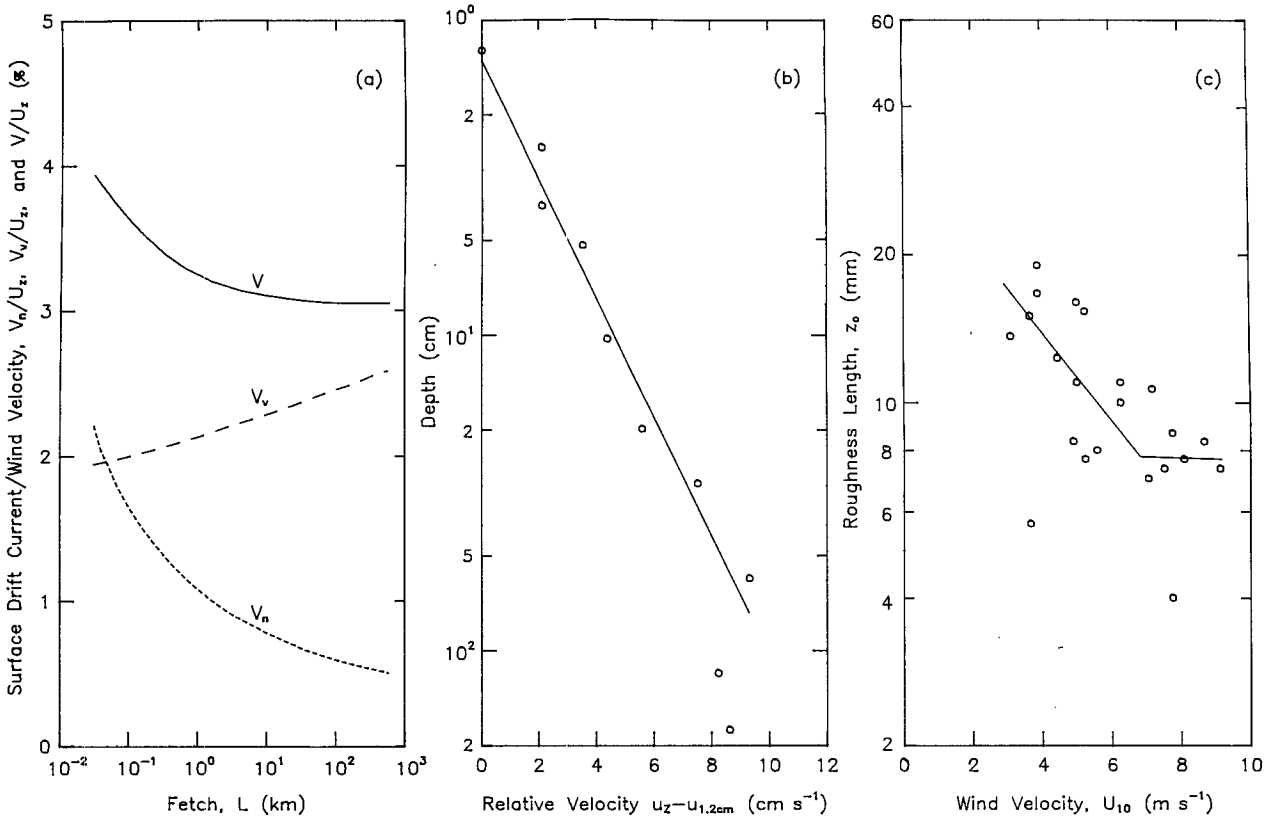

FIG. 1. Drift currents near the sea surface. The surface currents at $U_z = 10$ m s^{-1} are shown in (a), a sample vertical distribution of currents in (b), and roughness lengths at various wind velocities in (c). The results in (a) are from Wu (1983), and those in (b) and (c) from Churchill and Csanady (1983).

total drift current, L the fetch, and U_z the wind velocity at the reference height z above the mean sea surface; the latter is scaled according to the nondimensional fetch gL/U_z^2, where g is the gravitational acceleration. The surface current is seen to consist mainly of the wind-induced drift at short fetches and of the wave-induced transport at long fetches.

2) VERTICAL DISTRIBUTION OF DRIFT CURRENTS

Disk-shaped surface drifters and submerged drogues were used by Churchill and Csanady (1983) for measuring drift currents immediately below the sea surface. The drifter consisted of a slab of synthetic horsehair with a thin pad of microfoam glued to its top; the slab was square in shape, 20 cm on each side. Drifters of five different thicknesses: 2.4, 5.0, 7.6, 10.2, and 20.4 cm, were used; the top face of drifters was always at the sea surface. The drogue was made of a 40.5-cm diameter by 11-cm thick horsehair slab submerged at a specified depth and supported at the sea surface by a sealed plastic shell. The drogue and drifter were considered by Churchill and Csanady to follow the current at either the mean depth of the submerged drogue or one-half thickness of the surface drifter.

The measured currents were found to align nearly parallel to the wind and to the propagation of dominant waves; there was only a 10° deviation between the current at the shallowest depth of 1.2 cm and that at the deepest of 1.8 m. Vertically, the current confirmed the logarithmic distribution observed earlier by Wu (1975) in a wind wave tank with similar surface drifters and submerged drogues,

$$(U_s - u_z)/u_{*w} = (1/\kappa)\ln(z/z_0), \qquad (3)$$

where U_s and u_z are the currents at the sea surface and depth z, respectively; $u_{*w} = (\tau_w/\rho_w)^{1/2}$ is the friction velocity of currents, with τ_w being the current shear stress and ρ_w the water density; $\kappa = 0.4$ is the von Kármán universal constant; z_0 is the roughness length of aqueous boundary layer. A typical current profile shown in Fig. 8 of Churchill and Csanady is reproduced in Fig. 1b, where the velocity relative to that at the shallowest depth is presented. The logarithmic distribution of currents, indicated by the fitted straight line, is seen to extend to a depth of only about 1 m. Below this shallow interface layer, their vertical variation is much more gradual.

The friction velocities and roughness lengths of the aqueous boundary layer under various wind velocities

were obtained by Churchill and Csanady; the reported roughness lengths actually constitute the only set of field data available. The results presented in their Table 2 are in the form of roughness height, 30 z_0, versus the wind velocity at the 3-m elevation above the mean sea surface, U_3. The latter is converted herein to U_{10} at the 10-m elevation according to the logarithmic wind profile: $(U_{10} - U_3)/u_{*a} = (1/\kappa)\ln(10/3)$; the wind friction velocity in this expression can be obtained from

$$(u_{*a}/U_{10})^2 = C_{10} = (0.8 + 0.065\ U_{10}) \times 10^{-3}, \quad (4)$$

where C_{10} is the wind stress coefficient, of which the formula proposed by Wu (1980) is shown. The choice of such a formula is not critical for the present paper. The results are presented in Fig. 1c; the variation of roughness length with wind velocity is approximated by lines drawn in the figure. Except for two data points having much smaller values, the aqueous boundary layer is now seen to be hydrodynamically smooth for $U_{10} < 7$ m s^{-1}, where the roughness length decreases as the wind velocity increases. Beyond this wind velocity, the boundary layer becomes hydrodynamically rough, with the roughness length having nearly a constant value. Therefore, the vertical extent of strong shear currents also varies with the wind velocity; it increases rapidly first and then very slowly as the wind velocity increases. Interestingly enough, the atmospheric surface layer was found earlier to become aerodynamically rough also for $U_{10} > 7$ m s^{-1} (Wu 1981c).

b. Longitudinal dispersion process

Bubbles in the near-surface ocean are first produced below the breaker in an isolated plumelike structure (Koga 1982); it is called here the macrobubble cloud. Subsequently, bubbles in these isolated clouds are dispersed by combined actions of the longitudinal mean-flow convection and the lateral turbulent diffusion. This so-called longitudinal dispersion process was first established by Taylor (1954) for tracking an injected tracer in pipe flows; it was later extended by Elder (1959) to the dispersion of discrete particles in a wide channel. Subsequently, Wu (1969) applied their results to aqueous flows near the air–sea interface. As discussed earlier, the variation of these flows is principally in the vertical direction; it is represented by $u(z)$, shown as u_z in Eq. (3). The process in this case can be described by

$$\frac{\partial c}{\partial t} + u\frac{\partial c}{\partial x} = \frac{\partial}{\partial z}\left[\epsilon_z \frac{\partial c}{\partial z}\right], \quad (5)$$

where c is the concentration of material (bubbles) to be dispersed; t is the time following the injection of tracer (production of macrobubble cloud); x indicates the longitudinal axis along the wind direction; and ϵ_z is the eddy viscosity. As discussed earlier, the vertical extent of the interface layer is clearly displayed to be on the order of 1 m by the results of Churchill and Csanady (1983) shown in Figs. 1b, c. Both parameters u and c can be expressed as the sum of the cross-sectional average value spanning the interface layer and the deviation from this average:

$$u(x, z) = U(x) + u'(x, z),$$
$$c(x, z, t) = C(x, t) + c'(x, z, t). \quad (6)$$

Substituting Eq. (6) into Eq. (5), we obtain

$$\left(\frac{\partial c}{\partial t} + U\frac{\partial c}{\partial x}\right) + u'\frac{\partial c'}{\partial x} + u'\frac{\partial C}{\partial x} = \frac{\partial}{\partial z}\left(\epsilon_z \frac{\partial c'}{\partial z}\right). \quad (7)$$

The first and second terms on the left-hand side of the above expression represent, respectively, the substantive derivative of concentration with respect to time and the longitudinal derivative of the concentration variation; the third term represents the longitudinal variation of the mean concentration. It was demonstrated experimentally by Taylor (1954) and Elder (1959) that after the time t was large the first two terms were much smaller than the third. Consequently, the longitudinal dispersion process is seen to be dominated by the mean flow stretching the macrobubble cloud along the direction of the wind, and by the turbulent diffusion transferring bubbles laterally across the mean-velocity gradient.

In Elder's (1959) experiments, a tracer was suddenly injected into the water in the channel; the concentration of tracer was measured at various distances downstream from the injection point. The maximum concentration was found to move with the cross-sectional average velocity, $\bar{u}$; spatial distributions of the tracer concentration, both longitudinally and laterally, were found to be nearly Gaussian at the downstream distance $X = 50\ D/\bar{u}$, where D is the coefficient of longitudinal dispersion. From measured concentrations, the coefficient of longitudinal dispersion due to the combined action of turbulent lateral diffusion and mean-flow convection was determined to be 5.9 $u_{*w}H$, where H in the present case corresponds to the thickness of interface layer. Most importantly, this coefficient is about 26 times greater than that of turbulent lateral diffusion. Bubbles in the cluster immediately following their production by breaking waves can, therefore, be dispersed very efficiently by near-surface turbulent shear flows, discussed earlier.

In Thorpe's (1986) model of bubble dispersion, the current was considered to be uniform vertically, and turbulent diffusion was added independently. The longitudinal dispersion process, on the other hand, features the simultaneous actions of the shear-flow stretching and turbulent diffusion.

3. Formation of bubble layer

a. Critical observations of oceanic bubbles

Bubbles were measured earlier by Kolovayev (1976) with a trap in the subtropical ocean, and by Johnson

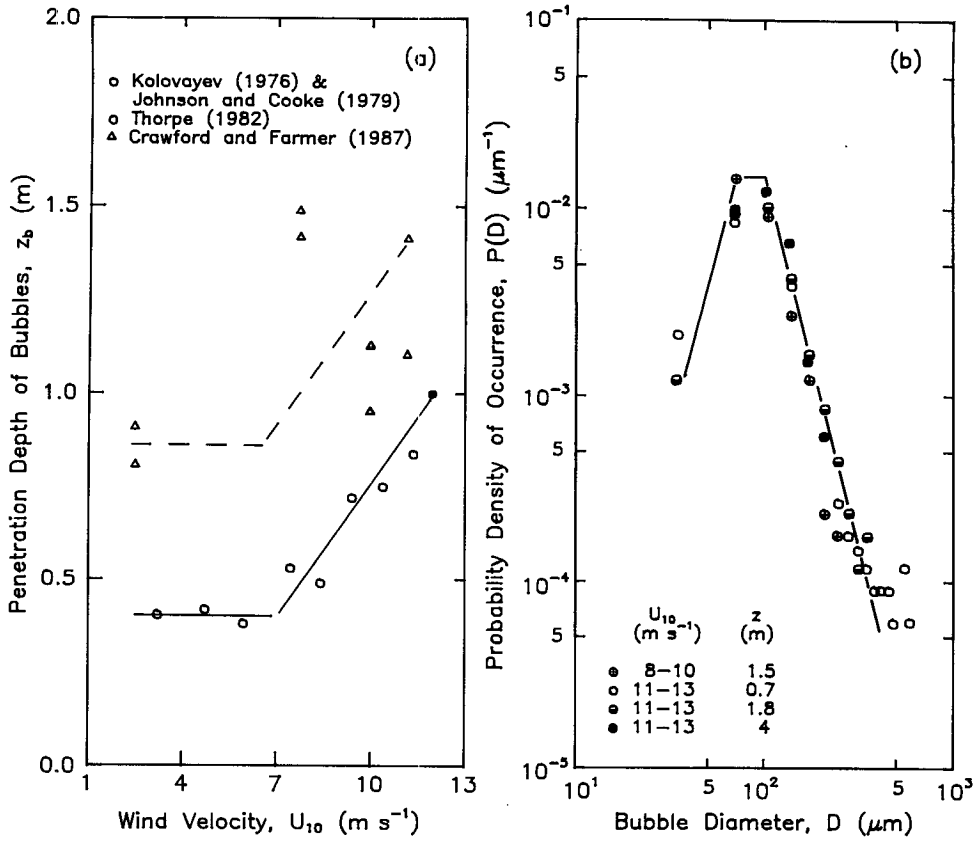

FIG. 2. Measurements of oceanic bubbles. The entrainment depths are reproduced from Wu (1992a) in (a), and the bubble spectrum from Wu (1992b) in (b).

and Cooke (1979) with a photographic technique in a coastal region. The acoustic scattering cross section, which is proportional to the bubble concentration, was measured subsequently at sea by Thorpe (1982). More recently, experiments were conducted offshore from Monterey, California, with an acoustic transducer by Crawford and Farmer (1987). In the meantime, a motor-driven camera was used by Walsh and Mulhearn (1987) to collect data in the Tasman Sea as well as the continental shelf. Measurements in these experiments conducted under various environmental conditions were parameterized earlier (Wu 1988a, 1992a); portions of these earlier results relevant to the present study are abstracted in the following.

1) VERTICAL DISTRIBUTION

The bubble populations at the sea surface for Kolovayev's and Johnson and Cooke's measurements were obtained by extrapolating their reported vertical distributions of bubble populations to zero depth (Wu 1981b). The bubble populations obtained by them at various depths were then normalized with the determined surface value, N_0; the normalized populations were found to decrease exponentially with depth

$$N(z)/N_0 = \exp(-z/z_b), \tag{8}$$

where z_b is a length characterizing the vertical entrainment of bubbles. The normalized acoustic cross sections, $M(z)/M_0$, measured by Thorpe were shown also to follow a similar variation (Wu 1988a). Such a distribution was verified by Crawford and Farmer, but not easily with Walsh and Mulhearn's data due to bubble populations at various depths being collected under different wind velocities.

The characteristic depths obtained from all these studies are reproduced from Wu (1992a) in Fig. 2a; the results of Kolovayev and of Johnson and Cooke are represented by a single data point obtained by Wu (1981b). The data of Thorpe (1982) are acoustic cross sections, not bubble populations, but the vertical distribution of their relative magnitudes was used to determine the characteristic length. Putting a slightly greater weight on the single data point representing the combined data of Kolovayev and of Johnson and Cooke and also more importantly the directly measured bubble population, the results shown in Fig. 2a were approximated by the solid line (Wu 1988a). The entrainment depths obtained by Crawford and Farmer were suggested (Wu 1992a) to follow a similar trend

but have somewhat larger values, indicating a more uniform vertical distribution of bubbles. It is not entirely clear whether this discrepancy could be attributed to the notion that bubbles detected by them might not be produced exclusively at the sea surface, although the biological production of bubbles was considered to be substantial at their experimental site (Wu 1981b). This may also represent the upper bound of bubble-layer thicknesses. The division of two regions at the wind velocity of 7 m s^{-1} was rationalized earlier to be associated with the transition of atmospheric surface-layer regimes. We note that with a side-scan sonar operated through an event with continuously increasing winds, Zedel and Farmer (1991) found the threshold wind velocity for the occurrence of penetrating bubble plumes also to be 7 m s^{-1}, at which the bubble layer is seen in Fig. 2a to thicken as the wind velocity increases. These isolated plumes penetrating beyond the bubble layer will be discussed in later sections.

2) BUBBLE SPECTRUM

Size spectra of bubbles obtained by Kolovayev and by Johnson and Cooke were normalized with their respective total bubble population to obtain the probability density distribution of bubbles of various sizes (Wu 1981b): $f_n(r) = n(z, r)/N(z)$, where $n(z, r)$ is the population of bubbles having the radius r at the depth z. For each investigation, the size spectra obtained at various depths under different wind velocities were found to be approximately invariant, having a similar shape but slightly different dropoffs on the large-diameter side. The difference of dropoffs was associated with the water temperature (Wu 1992a). The spectrum obtained from Johnson and Cooke's data is reproduced from Wu (1992b) in Fig. 2b.

b. Formation mechanisms of bubble layer

Taking together the results discussed above, physical processes of the generation and entrainment of bubbles are suggested. A macrobubble cloud is first generated by air entrained under the breaker; large bubbles soon return to the sea surface and burst. Small bubbles are then dispersed laterally into the interface layer, within which strong turbulent shear flows prevail. This is also confirmed by Crawford and Farmer (1987); they observed an almost continuous layer of bubbles near the sea surface. In the meantime, the current velocity in the interface layer is shown in Fig. 1b to follow the logarithmic distribution; this is then the constant-momentum-flux layer within which the friction velocity of currents is invariant. Such turbulent shear flows, as described below, are involved in two different physical processes for the formation of the bubble layer: bubble suspension and longitudinal dispersion. The production of the macrobubble cloud and the existence of bubble layer were also discussed by Monahan and Lu (1990); the main interest of the present article is in the mechanism of bubble-layer formation.

1) BUBBLE SUSPENSION

Results on the settling of solid particles in open-channel flows (Sumer 1977) were applied earlier to the suspension of spray droplets in the atmospheric surface layer (Wu 1982). The suspension of a water droplet in turbulent shear flows of the wind was considered to be governed by the parameter $\lambda = W/\kappa u_{*a}$, where W is the terminal fall velocity of the droplet. The droplet is likely to be suspended when λ has a value smaller than unity, of which various values between ¼ and 1 were suggested (Sumer 1977; Byutner 1978). Similarly, this criterion should be applicable to the rise of bubbles in turbulent shear currents near the sea surface. The terminal rise velocity of bubbles varies essentially with their diameter; in the meantime, the friction velocity of currents can be estimated from that of the wind as

$$u_{*w} = (\rho_a/\rho_w)^{1/2} u_{*a}. \tag{9}$$

Consequently, for values of λ = ¼ and ½, the critical diameters of bubbles at various wind velocities can be calculated (see Fig. 3). The upper bound of the value is lowered conservatively here to ½.

The critical diameter corresponding to the value λ = ¼ is seen in Fig. 3 to be nearly comparable with bubble diameters at which the size spectrum shown in Fig. 2b is peaked. At this λ value, the critical diameter for spray droplets in the atmospheric surface layer was also found to be comparable with the peak of their size spectrum (Wu 1982); these droplets, sampled far away from the sea surface, are very likely in a state of suspension. Taking together these results, the bubbles at and on the smaller diameter side of the spectral peak are also likely to be near a state of suspension. Oceanic

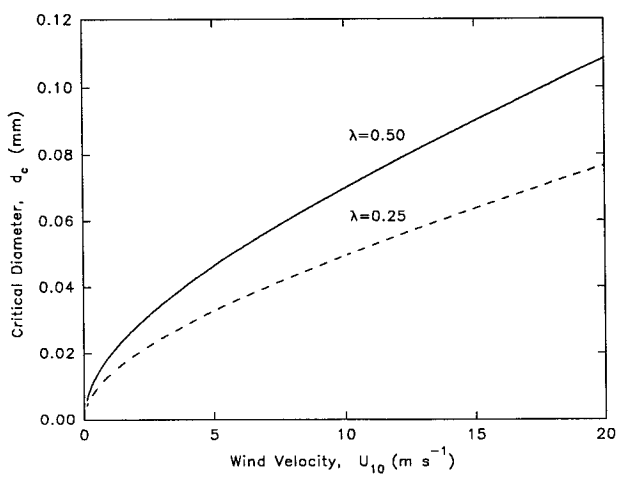

FIG. 3. Suspension of bubbles by turbulent shear flows near the sea surface.

observations (Crawford and Farmer 1987) also confirmed that these bubbles were detained in the shallow layer. Actually, the detainment for the present interest only has to be long enough (further discussed in the following section) to allow the longitudinal dispersion process to take its course.

2) LONGITUDINAL DISPERSION

It is primarily through shear flows of currents that the buoyancy effect on bubbles is suppressed. Consequently, the longitudinal dispersion process can distribute bubbles efficiently within the interface layer, as described earlier. Such a process, in fact, is clearly suggested by the proximity of two length scales: one characterizing the extension of turbulent shear flows shown in Fig. 1b, and the other the penetration of bubbles in Fig. 2a. Not only are these two scales comparable in magnitude, they also have a similar pattern of variations with the wind velocity, as shown in Figs. 1c and 2a. [The vertical extension of the flows as shown in Eq. (3) is scaled by the roughness length presented in Fig. 1c.] During the dispersion process, bubbles, of course, return continuously to the sea surface and burst (Blanchard 1963); an equilibrium presumably exists with bubbles being fully replenished by the action of breaking waves.

As discussed earlier, bubbles can be dispersed longitudinally within a traveling distance of $50\,D/\bar{u}$, where their spatial concentration is nearly Gaussian. Adopting the longitudinal dispersion coefficient determined by Elder (1959), we can estimate this distance for the 10 m s^{-1} wind as

$$X = 50\,D/\bar{u} = 50(5.9\,u_{*w}H)/\bar{u} = 18.4 \text{ m}, \quad (10)$$

in which $\bar{u} \approx 0.0155\,U_{10}$ (Fig. 1a), $H \approx 0.75$ m (Fig. 2a), and relationships shown in Eqs. (4) and (9) are substituted. The time required to complete this process is about $T = X/0.031\,U_{10} = 59$ s; this is only about nine dominant-wave periods. Both values, X and T, appear to be reasonably small for bubbles to be suspended and for the longitudinal dispersion process to complete its course.

Outside the interface layer, turbulent shear flows are too weak to suspend bubbles; there, the bubbles, if suspended, must be smaller in size and entrapped by other mechanisms.

4. Macrobubble clouds and microbubble plumes

a. *Macrobubble clouds*

The flows, induced by breaking waves, are quite similar to a jet impinging on the water surface (Koga 1982; Bonmarin 1989). Bubbles formed by the air entrained by such a jet are distributed by turbulent motions near the breaker to form a cloud below, and a whitecap on, the sea surface.

1) INDIVIDUAL CHARACTERISTICS

Oceanic data on sea surface whitecaps were analyzed by Wu (1992a) to obtain their spatial distribution and individual characteristics. Individual whitecaps were found from the data compiled by Bortkovskii (1987) to be generally wider along, than perpendicular to, the crest of breaking waves, with an aspect ratio being about 2.15. The area of individual whitecaps was found from the data of Snyder et al. (1983) to increase with the wind velocity

$$p = U_{10}^{1.6}/9, \quad (11)$$

where p is in meters squared. For example, at $U_{10} = 10$ m s^{-1} the area of typical whitecaps is about 4.4 m^2. Under each whitecap, there is a macrobubble cloud produced by the air entrainment through the wave breaking. The whitecap having the above area is then the base of macrobubble cloud.

The duration and intensity of wave breaking were found earlier (Hwang et al. 1989) to be closely related to the corresponding characteristics of breaking waves; consequently, the entrainment of bubbles was established to be governed by the breaking wave height, as discussed in Hwang et al. (1990). In the meantime, surface waves certainly play an important role for flows on the water side, whereas wave-induced components are generally negligible for airflows immediately above the sea surface, they are the major component of aqueous flows below as illustrated in Fig. 1a. Furthermore, the shallowness of the aqueous boundary layer displayed in Figs. 1b,c also indicates that the wave height appears to be more appropriate as the length scale of aqueous flows than the wavelength. For the case in hand, the disturbances of breaking waves and the penetration of bubble clouds were investigated by Bonmarin (1989) and Koga (1982). The bubble cluster was observed to extend downward by about one-half wave height, whereas individual bubbles were found to penetrate downward to about one wave height. Formulas of the significant wave height for fully developed seas were compared recently by Pierson (1991); the formula proposed by Sverdrup and Munk (1947) was found to provide the largest value and that by Ewing and Laing (1987) the smallest. These two formulas, in this order, are listed below:

$$H_{1/3} = 2.667 \times 10^{-2}\,U_{10}^2, \quad (12)$$

$$H_{1/3} = 8.7 \times 10^{-3}\,U_{10}^2 + 7.28 \times 10^{-4}\,U_{10}^3. \quad (13)$$

One-half the significant wave height, called here the significant wave amplitude $A_{1/3}$, is presented in Fig. 4 along with the bubble-layer thickness shown in Fig. 2a. Breaking waves in the field incept at wind velocities of about 3 to 4 m s^{-1} (Wu 1982); above these velocities, two quantities, z_b and $A_{1/3}$, are seen to be generally comparable. In other words, except at very low wind velocities, the macrobubble cloud appears to span ver-

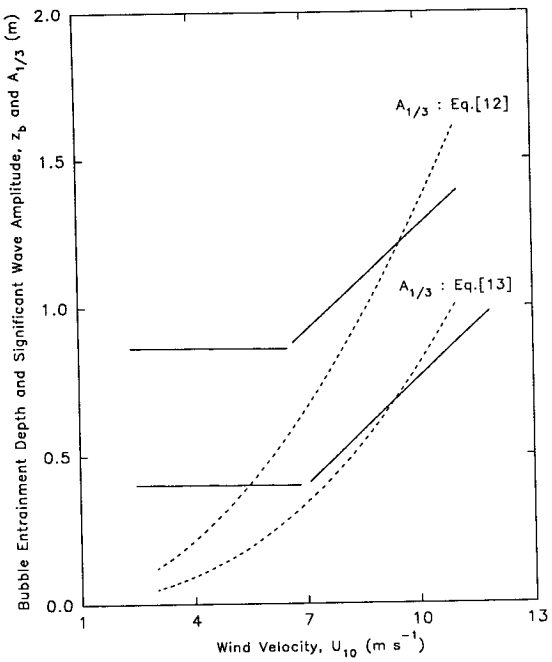

FIG. 4. Comparison between bubble entrainment depth and significant wave amplitude. The upper and lower bounds of the significant wave amplitude are shown as the dashed lines, while those of the entrainment depth are reproduced from Fig. 2a as solid lines.

tically the bubble layer. This is very interesting, as such a vertical structure is optimal for bubbles to be distributed by the longitudinal dispersion process. This also indicates that bubbles at greater depths are either those individual ones observed by Koga (1982) and Bonmarin (1989), or bubbles already in the layer being pushed downward by breaking waves. More on these bubbles will be discussed in a later section. It suffices to say that the macrobubble cloud appears to extend to the bottom of the bubble layer.

2) SPATIAL DISTRIBUTION

The fraction of sea surface covered by whitecaps was parameterized (Wu 1988b) from the data compiled by Monahan (1971), Monahan et al. (1981), and Doyle (1984) as $P = 2 \times 10^{-6}\, U_{10}^{3.75}$. Consequently, the area of sea surface within which there is a whitecap was found from this expression for the total coverage and Eq. (11) for individual areas (Wu 1992a):

$$P = 5.6 \times 10^{4}\, U_{10}^{-2.15}, \qquad (14)$$

where P is in m^2. Thus, it has a value of about 396 m^2 for $U_{10} = 10$ m s^{-1} being about two orders of magnitude greater than the area of individual whitecaps discussed earlier [Eq. (11)]. The typical lifetime of whitecaps was found to be about 3–4 s (Monahan and Zietlow 1969). Consequently, the whitecaps, and therefore the macrobubble clouds, are isolated spatially as well as temporally, because of their small dimensions and fleeting lives.

3) BUBBLE SIZES

Bubbles under spilling breakers were measured by Medwin and Breitz (1989) with an acoustical resonator floating at a fixed 25-cm depth below the sea surface. Their data acquired during winds of 12–15 m s^{-1} are reproduced in Fig. 5a. Three sets of data were reported. The group with the largest values, being about one order of magnitude greater than that with the smallest, was considered to be acquired under the breaker; the group with intermediate values was with breaking waves all around the instrument. Leaving out the group with the smallest values, Medwin and Breitz suggested that the spectral density followed a D^{-4} dropoff at smaller sizes, reached a narrow plateau at diameters of 100–125 μm, and then followed a $D^{-2.6}$ dropoff at larger sizes. They did not, however, suggest any physical basis for the plateau. Nonetheless, it is quite clear that the dropoffs at small and large bubble diameters, on either side of the "plateau," follow different trends. Two straight lines are then fitted to the data shown in Fig. 5a, ignoring the "plateau." The dropoff of spectral density is suggested to follow still D^{-4} at small sizes, but D^{-2} at large sizes. These two regions intersect at the bubble diameters of about 135–150 μm. The small-size region thus has a spectral shape similar to that shown in Fig. 2b for the bubble layer; the large-size region is suggested to represent the macrobubble cloud, to be further discussed in the following paragraph. Before the escape of large bubbles through the sea surface, the distribution of spectral densities inside the macrobubble cloud is more uniform, following a much more gradual dropoff. The data are quite scattered for the group having the smallest bubble concentrations; both segments, nevertheless, appear to follow the dropoff of D^{-4}.

The results shown in Fig. 5a are very interesting; the maximum and minimum concentrations can be interpreted to represent, respectively, bubbles at near and far fields of a breaker. Let us examine first the results for large sizes, $D > 150$ μm. The far field, corresponding to the bubble layer, is represented by the minimum-concentration group; quite consistently, the dropoff of the size spectrum follows D^{-4}. Whenever bubbles are produced freshly by breaking waves, they are superimposed upon those already in the bubble layer, causing an abrupt upward shift of the bubble concentration as illustrated in Fig. 5b. For conditions indicated by Medwin and Breitz with the sensor directly below the breaker, the maximum-concentration group is composed of bubbles in the macrobubble cloud and the bubble layer. With the presence of macrobubbles, the concentration follows a D^{-2} dropoff. Subsequently, the concentration of this group is lowered following the escape of large bubbles. Finally, the size spectrum is

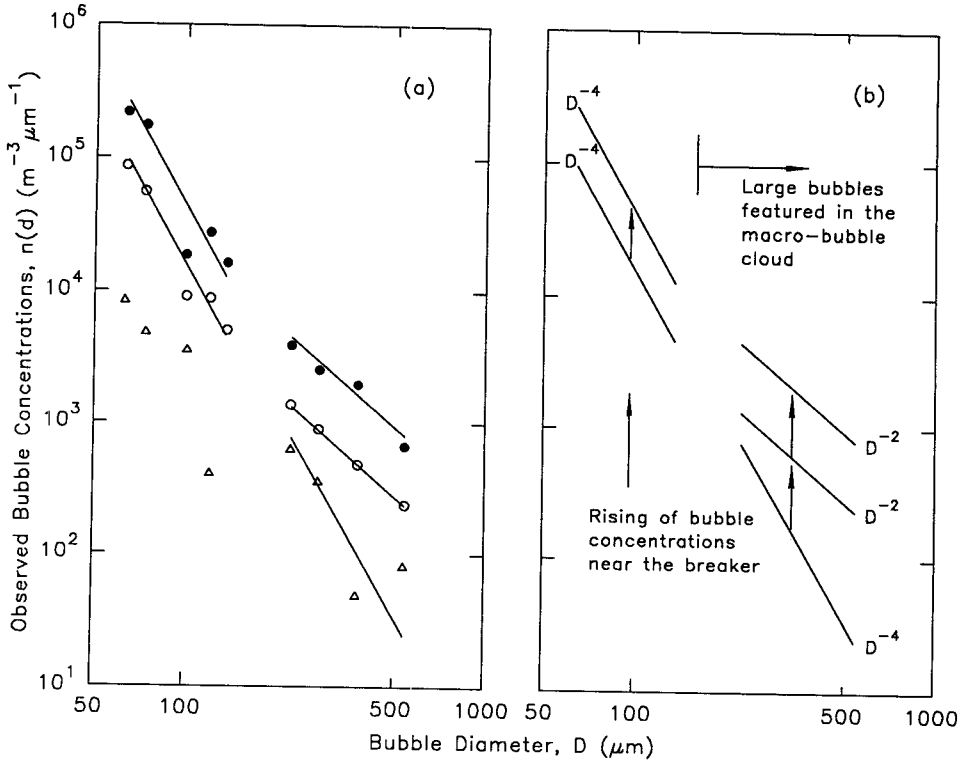

FIG. 5. Evolution of bubble spectrum illustrated by observations of Medwin and Breitz (1989). Their data inside (O) and outside (O) spilling breakers are shown in (a); the minimum values are also shown for the comparison.

seen to regain the spectral shape for the bubble layer. With breaking waves around the sensor, the intermediate concentrations measured by them still retained the near-field characteristics following the D^{-2} dropoff but as expected had lower values. Small bubbles were of course also produced by breaking waves, only the production of large bubbles there was disproportionally greater. Consequently, the elevated concentration is seen in Fig. 5a to retain the characteristic D^{-4} dropoff of the bubble layer. Most interestingly, the group representing the minimum concentrations at large sizes is only slightly above the extension of the group representing intermediate concentrations at small sizes. This indicates again the fast recovery of the bubble-layer structure following the transient intrusion of the macrobubble cloud. The macrobubble cloud obviously contains bubbles of all sizes. The concentration distributions in the large bubble diameter region are seen in Fig. 5a to display a very distinct pattern of superimposing the cloud onto the layer. Consequently, we tentatively suggest that the diameter of 150 μm divides bubbles featured in the cloud and the layer.

b. Microbubble plumes

1) PRODUCTION MECHANISM

The mechanism producing isolated plumes of small bubbles penetrating beyond the bubble layer is not entirely clear. As mentioned earlier, these deep bubbles are either the individual ones produced directly by breaking waves or the deflection of the bubble layer by breaking waves. Since these small bubbles have been observed to have plumelike structures (Thorpe 1986; Crawford and Farmer 1987), they are therefore unlikely those individual ones produced by breaking waves. On the other hand, such a structure can certainly be produced by pushing downward bubbles already in the layer, especially those near the lower boundary of the layer. Evidence for bubble entrainment by breaking waves, along with their observed features, are discussed in the following.

During the experiment of Thorpe and Humphries (1980), whitecaps were photographed and bubble plumes were detected by sonar; their results are reproduced in Fig. 6a. Similar variations of both phenomena with the wind velocity were stressed to indicate that the bubble plumes were most likely caused by breaking waves. However, the bubbles within the observed plume were not necessarily those produced freshly by breaking waves. They could be those near the lower boundary of bubble layer and carried further downward by breaking waves, as discussed above. In this case, the bubbles should be somewhat smaller than those dominant ones within the bubble layer, and therefore can be carried downward by the already weakened breaking action at that depth. The

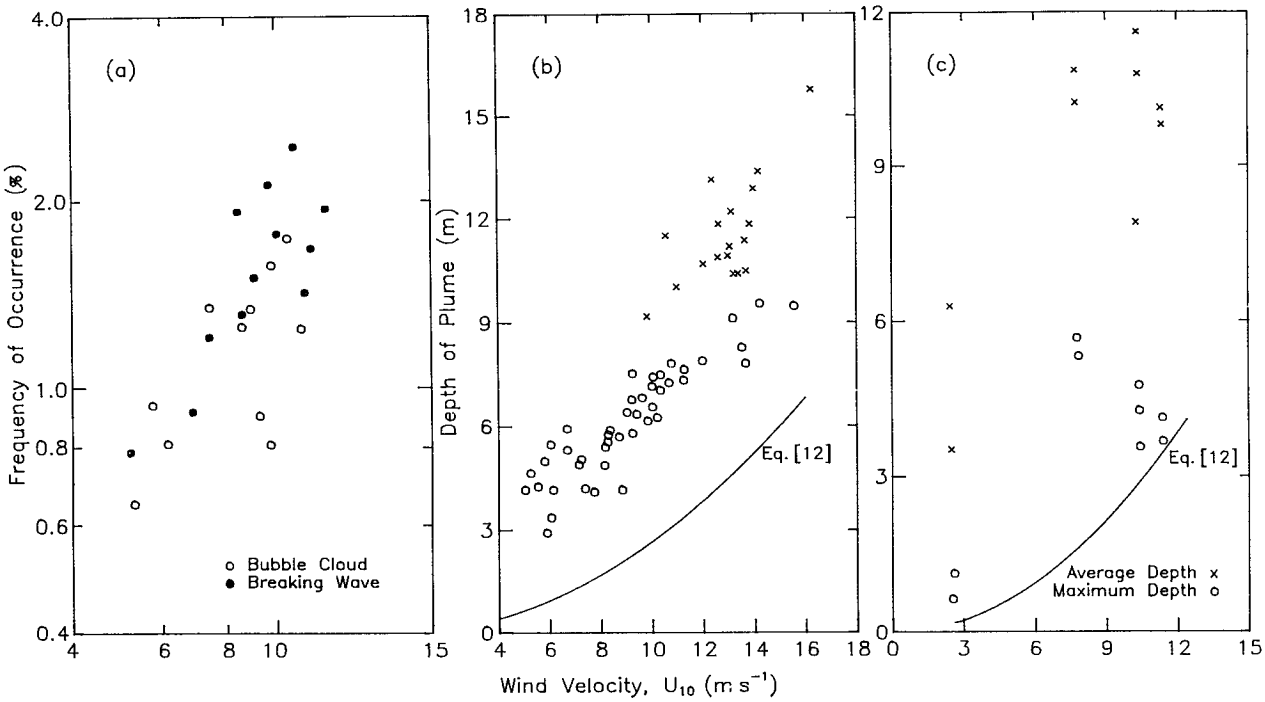

FIG. 6. Occurrences of breaking waves and bubble clouds obtained by Thorpe and Humphries (1980) are reproduced in (a), observed depths of bubble plumes by Thorpe (1986) in (b), and those by Crawford and Farmer (1987) in (c). The significant wave heights at various wind velocities are also shown in (b) and (c).

occurrence of bubble plumes being somewhat smaller than that of whitecaps was suggested by Thorpe and Humphries to be due to the fact that some waves did not produce bubbles. We would like to suggest another contributing factor that the disturbances caused by some breakers might not reach the lower boundary of the bubble layer. This factor may influence the use of upward-looking sonar to detect breaking waves.

Depths of plume penetration were reported by Thorpe (1986) and Crawford and Farmer (1987); their results are reproduced in Figs. 6b,c. The results of the latter investigation were already separated as the average and maximum depths of microbubble plumes. On the other hand, Thorpe's results were originally presented as one group; we see, however, that they can actually be divided into two groups and are therefore reproduced with different symbols. The significant wave height estimated according to Sverdrup and Munk's (1947) formula shown in Eq. (12), representing the larger of two values, is also diagrammed. The lower group of Thorpe's data and the average depth of Crawford and Farmer's are seen to be about double the significant wave height. The corresponding plumes were then about four times deeper than the bubble layer or the vertical extent of the macrobubble cloud. The plumes, nonetheless, could still be produced by breaking waves, as ocean waves are generally grouped (Donelan et al. 1972). The largest wave in the group can have an amplitude a few times greater than the significant wave height. More recently, observations were made by Zedel and Farmer (1991); they found that bubble plumes with an average penetration depth of about 6 m occurred when the wind velocity exceeded a threshold of approximately 7 m s^{-1}. They also pointed out that the presence of plumes was not accompanied by an increase of total volume of bubbles; the latter was correlated only with the wind speed. The observations are consistent with the concept advanced here.

As for those deeper plumes observed by Thorpe (1986) and Crawford and Farmer (1987), we are not certain about the mechanism of their productions. The larger-scale oceanic flows, such as those associated with oceanic fronts or the Langmuir circulation (Thorpe 1984), can certainly carry downward bubbles. Long, narrow bubble plumes aligned with the wind were observed by Thorpe (1986) and Zedel and Farmer (1991); these plumes were also found to follow the structure of windows caused by Langmuir circulation. Undoubtedly, the latter can redistribute most efficiently bubbles already dispersed into the layer. As discussed earlier, this initial dispersion can be completed within a few periods of breaking waves. This result is also clear from observations showing deeper plumes that were accompanied by a persistent bubble layer.

2) BUBBLE SIZE

The size of bubbles associated with microbubble plumes produced by breakers can be as large as those

at the spectral peak shown in Fig. 2b. As suggested above, most bubbles in these isolated plumes are those already suspended in the bubble layer. On the other hand, the bubbles carried downward by other oceanic flows are likely to be much smaller; they are very likely those on the small-diameter side of the spectrum, starting at the diameter of about 50 μm. Bubbles in this category were suggested by Crawford and Farmer (1987) to act as passive contaminants in the water column, having negligible buoyancy.

5. Concluding remarks

The existence of the bubble layer was suggested earlier (Wu 1981b); subsequently, its structure and composition were related to the wind velocity (Wu 1988a). More recently, its existence was further confirmed by observations (Zedel and Farmer 1991). Here, the mechanism of its generation is provided; the bubbles within the layer are nearly suspended by turbulent shear flows and distributed by the longitudinal dispersion process. On the basis of these results and those of sea surface whitecaps, structures of both macrobubble clouds and microbubble plumes are discussed. The macrobubble cloud is isolated specially, and appears to span vertically the bubble layer. The shallower microbubble plumes are believed to be generated through the deflection of the bubble layer by breaking waves, while the deeper ones are generated by other oceanic flows. Langmuir circulation is certainly important for the deeper structures of bubbles; the longitudinal dispersion discussed herein, however, is much more effective in dispersing the macrobubble cloud into a layer. We also like to note that aqueous flows immediately below the sea surface have been systematically measured by only Churchill and Csanady (1983); the well-observed bubble layer can also be interpreted to confirm their results on very intensified but shallow turbulent shear flows near the sea surface.

Acknowledgments. I am very grateful for the support of this work provided by the Ocean/Atmospheric/Polar Environments Program (Contract N00014-87-K-1557), Office of Naval Research.

REFERENCES

Blanchard, D. C., 1963: The electrification of the atmosphere by particles from bubbles in the sea. *Progress in Oceanography,* Vol. 1, Pergamon Press, 71–202.

——, and A. H. Woodcock, 1957: Bubble formation and modification in the sea and its meteorological significance. *Tellus,* **9,** 145–158.

Bonmarin, P., 1989: Geometric properties of deep-water breaking waves. *J. Fluid Mech.,* **209,** 405–433.

Bortkovskii, R. S., 1987: *Air–Sea Exchange of Heat and Moisture During Storms.* D. Reidel.

Byutner, E. K., 1978: *The Dynamics of the Atmospheric Surface Layer.* Gidrometeoizdat, Leningrad.

Churchill, J. H., and G. T. Csanady, 1983: Near-surface measurements of quasi-Lagrangian velocities in open water. *J. Phys. Oceanogr.,* **13,** 1669–1680.

Crawford, G. B., and D. M. Farmer, 1987: On the spatial distribution of ocean bubbles. *J. Geophys. Res.,* **92,** 8231–8243.

Donelan, M. A., M. S. Longuet-Higgins, and J. S. Turner, 1972: Periodicity in whitecaps. *Nature,* **239,** 449–450.

Doyle, D. M., 1984: Marine aerosol research in the Gulf of Alaska and on the Irish west coast (Inishmore). Whitecaps and the Marine Atmosphere Report 6, University College, Galway, Ireland.

Elder, J. W., 1959: The dispersion of marked fluid in turbulent shear flow. *J. Fluid Mech.,* **5,** 544–560.

Ewing, J. A., and A. K. Laing, 1987: Directional spectra of seas near full development. *J. Phys. Oceanogr.,* **17,** 1696–1706.

Farmer, D. M., and S. Vagle, 1989: Wave guide propagation of ambient sound in the ocean-surface bubble layer. *J. Acoust. Soc. Am.,* **86,** 1897–1908.

Hwang, P. A., D. Xu, and J. Wu, 1989: Breaking of wind-generated waves: Measurements and characteristics. *J. Fluid Mech.,* **202,** 177–200.

——, Y.-H. L. Hsu, and Jin Wu, 1990: Air bubbles produced by breaking wind waves: A laboratory study. *J. Phys. Oceanogr.,* **20,** 19–28.

Johnson, B. D., and R. C. Cooke, 1979: Bubble populations and spectra in coastal waters: A photographic approach. *J. Geophys. Res.,* **84,** 3761–3766.

Koga, M., 1982: Bubble entrainment in breaking wind waves. *Tellus,* **34,** 481–489.

Kolovayev, P. A., 1976: Investigation of the concentration and statistical size distribution of wind-produced bubbles in the near-surface ocean layer (English translation). *Oceanology,* **15,** 659–661.

McDaniel, S. T., and A. Gorman, 1983: Spectral spread of sea-surface reverberation. *J. Acoust. Soc. Am.,* **74,** 241–248.

Medwin, H., and N. D. Breitz, 1989: Ambient and transient bubble spectral densities in quiescent seas and under spilling breakers. *J. Geophys. Res.,* **94,** 12 751–12 759.

Merlivat, L., and L. Memery, 1983: Gas exchange across an air–water interface: Experimental results and modeling of bubble contribution to transfer. *J. Geophys. Res.,* **88,** 707–724.

Monahan, E. C., 1971: Oceanic whitecaps. *J. Phys. Oceanogr.,* **1,** 139–144.

——, and C. R. Zietlow, 1969: Laboratory comparisons of fresh-water and salt-water whitecaps. *J. Geophys. Res.,* **74,** 6961–6966.

——, and M. Lu, 1990: Acoustically relevant bubble assemblages and their dependence on meteorological parameters. *IEEE J. Oceanic Eng.,* **15,** 340–349.

——, I. G. Muircheartaigh, and M. P. FitzGerald, 1981: Determination of surface wind speed from remotely measured whitecap coverage—A feasibility assessment. European Space Agency SP-167, 103–109.

Pierson, W. J., Jr., 1991: Comments on "Effects of sea maturity on satellite altimeter measurements" by R. E. Glazman and S. H. Piloz. *J. Geophys. Res.,* **96,** 4973–4977.

Snyder, R. L., L. Smith, and R. M. Kennedy, 1983: On the formation of whitecaps by a threshold mechanism. Part III: Field experiment and comparison with theory. *J. Phys. Oceanogr.,* **13,** 1505–1518.

Stokes, G. G., 1847: On the theory of oscillating waves. *Trans. Cambridge Phil. Soc.,* **8,** 441–445.

Sumer, B. M., 1977: Settlement of solid particles in open-channel flow. *ASCE J. Hydraul. Div.,* **103,** 1323–1337.

Sverdrup, H. U., and W. H. Munk, 1947: Wind seas and swell: Theory of relationships for forecasting. Publication 601, Navy Hydrographic Office, Washington, D. C.

Taylor, G. I., 1954: The dispersion of matter in turbulent flow through a pipe. *Proc. Roy. Soc. London,* **A223,** 446–468.

Thorpe, S. A., 1982: On the clouds of bubbles formed by breaking wind-waves in deep water, and their role in air–sea gas transfer. *Philos. Trans. Roy. Soc. London,* **A304,** 155–210.

——, 1984: The effect of Langmuir circulation on the distribution of submerged bubbles caused by breaking wind waves. *J. Fluid Mech.*, **142**, 151–170.
——, 1986: Measurements with an automatically recording inverted echo sounder; ARIES and the bubble clouds. *J. Phys. Oceanogr.*, **16**, 1462–1478.
——, and P. N. Humphries, 1980: Bubbles and breaking waves. *Nature*, **283**, 463–465.
Walsh, A. L., and P. J. Mulhearn, 1987: Photographic measurements of bubble populations from breaking wind waves at sea. *J. Geophys. Res.*, **92**, 14 553–14 565.
Wu, J., 1969: An estimation of wind effects on dispersion in wide channels. *Water Resour. Res.*, **5**, 1097–1104.
——, 1975: Wind-induced drift currents. *J. Fluid Mech.*, **68**, 49–70.
——, 1980: Wind-stress coefficients over sea surface near neutral conditions—A revisit. *J. Phys. Oceanogr.*, **10**, 727–740.
——, 1981a: Evidence of sea spray produced by bursting bubbles. *Science*, **212**, 324–326.
——, 1981b: Bubble populations and spectra in near-surface ocean: Summary and review of field measurements. *J. Geophys. Res.*, **86**, 457–463.
——, 1981c: On critical roughness Reynolds numbers of the atmospheric surface layer. *J. Geophys. Res.*, **86**, 6661–6665.
——, 1982: Sea spray: A further look. *J. Geophys. Res.*, **87**, 8905–8912.
——, 1983: Sea-surface drift currents induced by wind and waves. *J. Phys. Oceanogr.*, **13**, 1441–1451.
——, 1988a: Bubbles in the near-surface ocean—A general description. *J. Geophys. Res.*, **93**, 587–590.
——, 1988b: Variation of whitecap coverage with wind stress and water temperature. *J. Phys. Oceanogr.*, **18**, 1448–1453.
——, 1992a: Individual characteristics of whitecaps and volumetric description of bubbles. *IEEE J. Oceanic Eng.*, **17**, 150–158.
——, 1992b: Bubble-flux and marine aerosol spectra under various wind velocities. *J. Geophys. Res.*, **97**, 2327–2333.
Zedel, L., and D. Farmer, 1991: Organized structures in subsurface bubble clouds: Langmuir circulation in the open ocean. *J. Geophys. Res.*, **91**, 8889–8900.

CORRIGENDUM

Authors Alexander V. Soloviev and Peter Schlüssel have noted several typographical errors in their article "Parameterization of the cool skin of the ocean and of the air–ocean gas transfer on the basis of modeling surface renewal" that appeared in the June 1994 issue of the *Journal of Physical Oceanography*, Vol. 23, No. 6, pages 1339–1346. On page 1342, right column, the corrections are as follows.

$$\Delta\bar{T} = \Lambda_0 \,\mathrm{Pr}^{1/2}(-\alpha g q_0^{-3}\nu/Rf_{cr})^{-1/4} \tag{27}$$

(The last exponent is $-1/4$.)

$$K = A\Lambda_0^{-1}\,\mathrm{Sc}^{-1/2}(-\alpha g q_0 \nu/Rf_{cr})^{1/4} \tag{28}$$

(The exponent -3 is deleted.)

In text following (28) the equation at end of the paragraph is

$$b = \Lambda_0(-Rf_{cr})^{1/4}$$

(The exponent is $1/4$.)

In the next paragraph

$$\Delta\bar{T} = \Lambda_0 \,\mathrm{Pr}^{1/2}(\nu g\,\mathrm{Ke}_{cr})^{-1/2} q_0 u_*^{1/2} \tag{31}$$

(The middle exponent is $-1/2$.)

$$K = A\Lambda_0^{-1}\,\mathrm{Sc}^{-1/2}(\nu g\,\mathrm{Ke}_{cr})^{1/2} u_*^{-1/2} \tag{32}$$

(Delete the minus sign, $K = A\cdots$.)

The errors are typographical and do not change the conclusions of the paper.

The authors are grateful to Kimberly van Scoy for pointing out these errors.